Geophys. J. Int. (2006) **164,** 551–568 doi: 10.1111/j.1365-246X.2006.02861.x

On the use of teleseismic receiver functions for studying the crustal structure of Iceland

Vera Schlindwein*

Department of Geological Sciences, University of Durham, Durham, UK

Accepted 2005 November 2. Received 2004 June 24; in original form 2001 March 15

SUMMARY

The character of the crust–mantle transition beneath Iceland, a ridge-centred hotspot, is not well known despite a wealth of geophysical data including recent seismic refraction profiles. From scattered observations of a 20–40-km-deep seismic reflector and *Pn* velocities of 7.7–8.0 km s^{-1}, it has been concluded that the Icelandic crust is 20–40 km thick and solid, underlain by solid upper mantle. Receiver functions are sensitive to seismic velocity contrasts and, therefore, well suited to study the proposed Moho. Several receiver function studies have been conducted meanwhile, but they show only weak *P–S* converted phases, which proved difficult to interpret. An intensive analysis of the receiver function signals and a comparison of the results with those of other receiver function studies shows that the value of the receiver function technique for studying the crust–mantle transition underneath Iceland is limited. A rapid velocity increase in the upper 8–14 km of the crust, underlain by almost constant velocities below, accounts for much of the first 1–4 s of the receiver function signals, potentially masking phases from a Moho. Therefore, 1-D velocity profiles obtained by receiver function inversion were tested intensively by forward modelling to check the robustness of the results. Receiver function analysis of 28 sites in Iceland, equipped with broad-band seismometers during the HOTSPOT project from 1996 June to 1998 July, showed that a ubiquitous prominent Moho velocity contrast does not offer a good match of the observed receiver function signals. Instead, the character of the crust–mantle transition varies from not being detectable, to gradient zones, and discrete velocity discontinuities. A tendency to reduced *S* velocities is observed at about 40 km depth beneath central Iceland. By comparison with other studies, I tentatively interpret this low-velocity zone as an indication of a shallow asthenosphere.

Key words: crustal structure, Iceland, mantle plume, receiver function, waveform analysis.

INTRODUCTION

The crustal structure of Iceland, an oceanic island situated above a ridge-centred hotspot, has been debated for several decades (e.g. Gudmundsson 1994; Bjarnason *et al.* 1994). Kaban *et al.* (2002) give a recent summary of geophysical observations stressing that no model has yet been found that consistently explains all data. A first model considered the crust beneath Iceland as anomalously hot, only 10–15 km thick, and underlain by partially molten mantle (e.g. Angenheister *et al.* 1980; Gebrande *et al.* 1980). A high-conductivity layer at about the same depth identified from magnetotelluric studies (Beblo & Björnsson 1980; Eysteinsson & Hermance 1985) and high surface heat flow (Pálmason 1973; Flóvenz & Sæmundsson 1993) seemed to support this model. However, since the 1990s, a number of long seismic refraction lines showed wide-angle reflections from a 20–40-km-deep reflector that was interpreted as representing the Moho (e.g. Bjarnason *et al.* 1993; Staples *et al.* 1997; Darbyshire *et al.* 1998; Menke *et al.* 1996, 1998). Refracted head waves arising from this interface have rarely been observed, but Bjarnason *et al.* (1993), for example, reported arrivals from about 25 km depth with apparent velocities of 7.5–7.7 km s^{-1}, which they interpreted as a *Pn* phase. Observed *Vp*/*Vs* ratios of 1.76–1.79 (e.g. Menke *et al.* 1994) suggest that partial melt is not present above 20–35 km depth. Hence, in the second model the crust is considered to be solid, relatively cool and 20–40 km thick. This thick crust partly accounts for the gravity low in the centre of Iceland, which is further caused by high-temperature and low-density material in the centre of the mantle plume beneath Iceland (Gudmundsson 2003; Kaban *et al.* 2002; Darbyshire *et al.* 2000b). Finally, crustal thicknesses of 20–40 km can be produced by melt extraction during passive decompression of an anomalously hot mantle (e.g. Bown & White 1994).

Despite these recent observations in favour of a thick and cool crust, the character of the crust–mantle transition remains

*Now at: Alfred Wegener Institute for Polar and Marine Research, Columbusstrasse, D 27568 Bremerhaven, Germany. E-mail: vschlindwein@awi-bremerhaven.de.

poorly known. A common problem of seismic refraction studies in Iceland is to constrain the seismic velocities in the lower crust and upper mantle as few observations of refracted waves with turning points at these depths are available. Values proposed for the velocity contrast across the Moho vary from 0.3 km s^{-1} (Bjarnason *et al.* 1993) to at least 0.9 km s^{-1} (Staples *et al.* 1997) at different places. This may reflect the uncertainties of the refraction results, crustal heterogeneity or a combination of both. Gravity modelling suggests that the density contrast across the crust–mantle boundary is small with abnormally high densities in the lower crust (Gudmundsson 2003). In addition, PmP reflections from the Moho are seldom observed over a wide offset range suggesting a non-continuous Moho interface, which may also show pronounced topography (e.g. Staples *et al.* 1997; Darbyshire *et al.* 1998).

Recently, efforts have been made to study in detail the nature of the crust–mantle transition in Iceland using teleseismic receiver functions. The studies of Du & Foulger (1999, 2001) and Du *et al.* (2002) are referred to hereafter as DF, and the study of Darbyshire *et al.* (2000a) as DA. Receiver functions are very sensitive to velocity contrasts in the subsurface beneath a seismic recording site. The *P* waves from teleseismic earthquakes impinge on receiver stations from directions close to the vertical. *P–S* mode-converted phases are generated at the Moho or at crustal interfaces. The radial receiver function isolates these converted phases (e.g. Langston 1979) and allows the traveltimes from the interfaces to the surface to be determined. The amplitudes of the converted phases are sensitive to the impedance contrasts at the interfaces. However, it is not possible to obtain information on absolute seismic velocities and depths of interfaces simultaneously due to the inherent trade-off between these parameters.

Receiver function studies are a robust technique, widely used to image and characterize the nature of the Moho in both continental regions (e.g. Kosarev *et al.* 1999) and oceanic settings. Li *et al.* (2000), for example, imaged the Moho and mantle discontinuities beneath Hawaii. However, the use of receiver functions in Iceland has proved difficult and has given rise to partly conflicting results (DF; DA). Problems arise from strong crustal heterogeneity, weak and incoherent converted phases, high levels of microseismic noise and the inherent non-uniqueness of receiver function inversion. However, the results of the receiver function studies are used in further studies to fill in gaps in the estimates of the Moho depth between the refraction profiles (e.g. Darbyshire *et al.* 2000b; Gudmundsson 2003). Hence a careful assessment of the ability of receiver functions to constrain the crustal thickness of Iceland and of the reliability of the results is urgently needed.

In this paper, I present the results of a comprehensive receiver function study of Iceland at 28 receiver sites distributed over all Iceland. The study has been conducted independently of DF using the same basic data but different processing strategies. This study, therefore, offers an excellent opportunity to test the influence of the analyst and the methodological approach on the proposed results and hence to demonstrate the capabilities and limitations of the method. I focus on the potential of the receiver functions to detect the Moho beneath Iceland comparing the results intensively with previous receiver function results (DF; DA). The receiver function models presented here give further a weak hint of a low-velocity layer below the crust in central Iceland at about 40 km depth, whereas this layer appears to be absent in West and East Iceland.

CALCULATION OF RECEIVER FUNCTIONS

Method

The HOTSPOT project, a passive seismology experiment, was designed to gain insight into the crustal structure of Iceland and to study the mantle plume beneath Iceland (e.g. Allen *et al.* 1999; Du & Foulger 1999). From 1996 June to 1998 July, a network of 35 PASSCAL broad-band seismometers distributed throughout Iceland continuously recorded seismic events. The seismometer stations were equipped with Guralp three-component seismometers (mostly with CMG-3ESP seismometers; four stations with CMG-40T; one station with CMG-3T) and Refraction Technology 72a-02 24-bit data loggers sampling at a rate of 20 Hz. All seismometers had a flat response to particle velocity for frequencies in the range 0.09–100 Hz. The vertical and horizontal components present similar instrument responses (Du & Foulger 1999). Absolute timing was provided by GPS clocks. Regular maintenance was difficult for remote stations, which resulted in periods of lost data. However, 28 of the stations recorded a sufficient number of high-quality signals suitable for receiver function analysis (Fig. 1).

Receiver functions are calculated from the *P* coda of strong earthquakes with near-vertical incidence at the receiver station. About 100 teleseismic events at epicentral distances of 30°–90° with magnitudes in excess of 5.8 were considered. To limit problems related to high levels of microseismic noise in Iceland (e.g. Du & Foulger 1999), only teleseismic events with detectable *P*-phase onsets in the unfiltered raw data were selected. This considerably reduced the usable data set. The horizontal components were rotated into radial and transverse directions using the coordinates of each station-epicentre pair. The particle motion of the *P* phase in the horizontal plane was inspected and, if necessary, the rotation adjusted to minimize the seismic energy on the transverse component.

The radial and transverse receiver functions are obtained by deconvolving the vertical component seismogram of a teleseismic event from the radial and transverse component seismograms, respectively, using the frequency domain source equalization method of Langston (1979). A full review of the method can be found in Cassidy (1992). A water-level parameter of 0.003 and a Gaussian filter removing frequencies higher than ∼0.5 Hz (e.g. Cassidy 1992) were selected. I used the refined algorithm of Ammon (1991) to calculate the receiver functions as it preserves the absolute amplitudes of the receiver functions.

Receiver functions were excluded from further study if the pre-signal noise level was too high or the amplitudes of the transverse receiver functions were larger than the corresponding radial receiver functions. Radial receiver functions with waveforms greatly differing from the majority of the waveforms at one station were rejected. In this way, the data set was reduced to 26 teleseismic events, which yielded high-quality receiver functions at most stations. These were clustered in three limited source regions, referred to hereafter as N, E and WSW (Table 1).

To enhance the main signal characteristics, several receiver function stacks and their standard deviations were calculated (Fig. 2). The stack of all the receiver functions selected for a station shows the most prominent signal features, but details are lost in averaging. Comparison of the stacks of the events from the three different source regions provides information on azimuthal variation of the receiver functions and, hence, of the crustal structure. Events

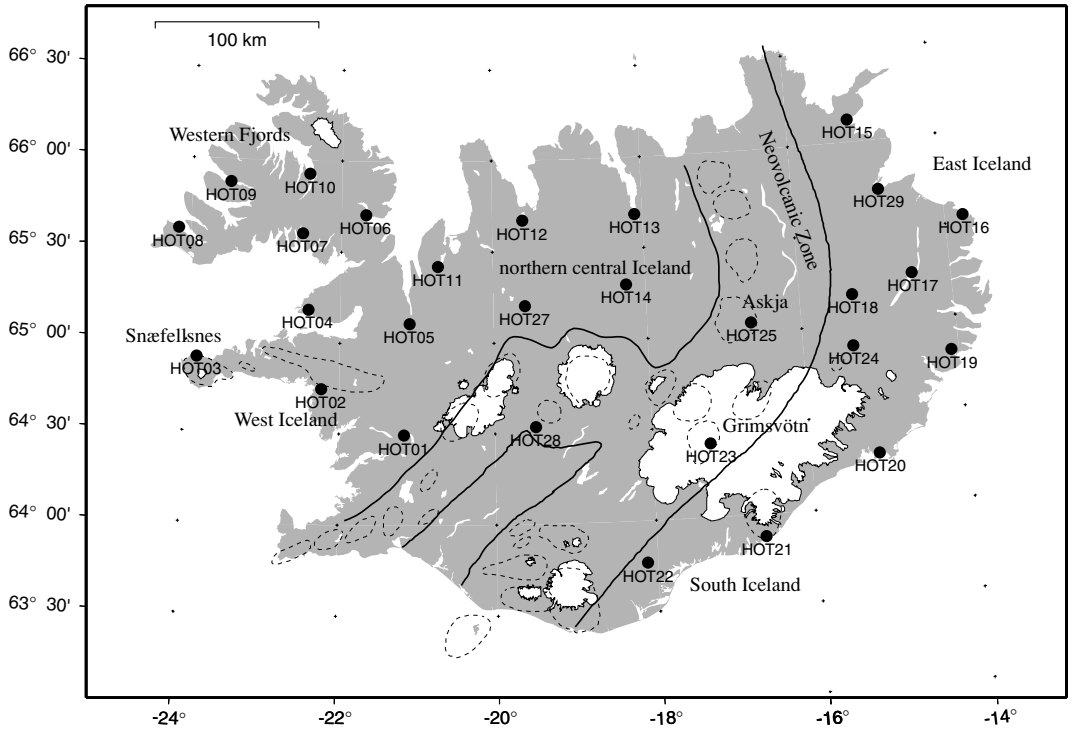

Figure 1. Map of Iceland showing the locations of the seismometer sites of the HOTSPOT project. The NVZ includes the mid-Atlantic plate boundary. The crust ages away from the rift zone and reaches maximum ages of 10–15 Ma in East Iceland and the Western Fjords. Snæfellsnes represents a zone of flank volcanism. Dashed lines show recent volcanic centres (Jóhannesson & Sæmundsson 1998) and white areas the icecaps.

Table 1. Teleseismic events used for receiver function calculation.

Event No	Origin time YYYY DDD HH:MM:SS	Epicentral distance (HOT01)	Backazimuth (HOT01)	Magnitude depth	Stack [km]	
1	1997 339 11:32:17	60.5	358.0	7.7	33	N
2	1997 339 18:53:52	61.6	358.3	6.5	33	N
3	1998 152 05:39:40	62.6	359.2	6.3	40	N
4	1996 173 14:02:53	63.9	359.8	6.6	20	N
5	1998 123 23:38:26	89.4	30.7	7.3	33	N
6	1996 249 23:50:10	88.9	34.3	6.6	20	N
7	1997 195 16:16:08	71.5	8.8	6.0	33	N
8	1996 357 14:59:54	70.6	14.3	6.0	227	N
9	1997 225 04:52:59	85.5	31.1	6.0	55	N
10	1996 324 10:50:15	62.3	65.4	7.1	33	E
11	1997 141 22:58:14	73.9	69.9	6.0	36	E
12	1997 133 14:18:48	58.4	70.5	6.1	196	E
13	1998 150 06:27:24	57.5	70.9	6.9	33	E
14	1997 130 08:02:18	56.2	81.7	7.3	33	E
15	1997 286 13:42:07	38.1	116.4	6.6	24	
16	1996 283 13:14:11	44.1	106.0	6.8	33	
17	1998 178 13:59:03	43.6	101.3	6.2	33	
18	1997 322 13:10:04	37.0	117.7	6.4	33	
19	1998 142 04:57:04	88.9	221.7	6.6	24	WSW
20	1997 190 19:29:49	61.5	228.9	6.8	20	WSW
21	1997 245 12:20:08	72.0	238.8	6.4	232	WSW
22	1996 317 17:08:02	89.3	230.9	7.3	33	WSW
23	1997 142 07:57:20	68.6	268.7	6.0	70	WSW
24	1997 121 11:44:15	70.2	272.4	6.7	33	WSW
25	1997 301 06:22:46	79.8	235.3	6.5	125	WSW
26	1997 200 14:28:41	72.7	270.2	6.3	33	WSW

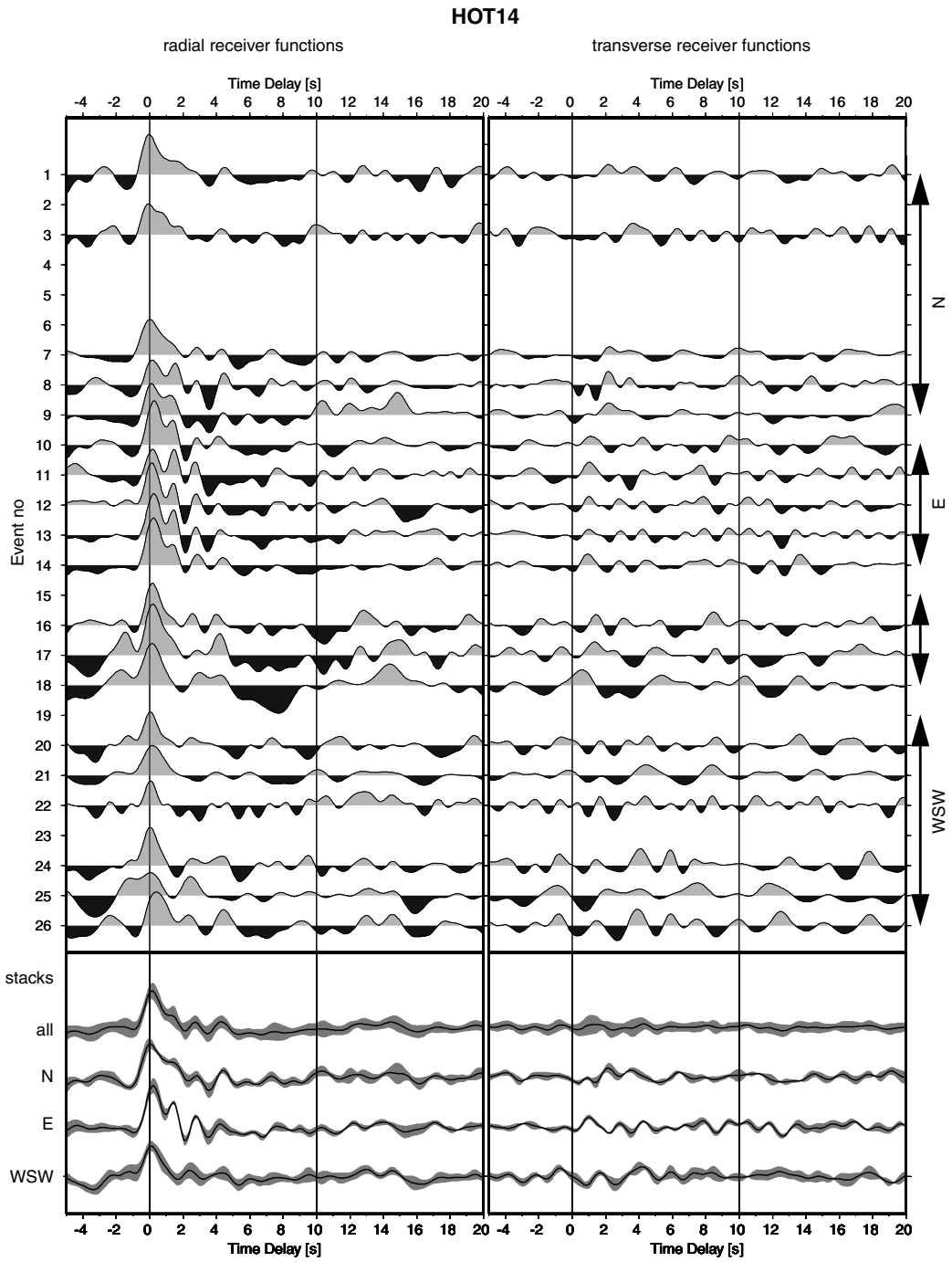

Figure 2. Example of individual receiver functions and their stacks (solid line) with standard deviation (grey shading) for station HOT14. Some events (see Table 1) were not recorded. The stack of all receiver functions shows the most prominent parts of the signal, whereas the azimuthal variation of the signal is seen by comparing the N, E and WSW stacks. Note the sequence of equidistant peaks at 2–5 s time delay and a coherent phase at 13–15 s.

15–18 were omitted from the E stacks as their epicentral distances are considerably smaller than those of events 10–14 resulting in different waveforms (Table 1). The latter yielded the best-quality receiver functions as can be seen from narrow standard deviation bounds, low noise level and good signal coherency (Fig. 2). In addition, as the stack contains events from a narrow backazimuth (16°) and distance range (18°), loss of information by averaging the crustal properties over a large area is avoided.

The radial receiver functions contain a contribution from the direct *P* phase, which can be seen in the radial component seismogram since the incident ray paths are inclined at angles of 10°–25° to the vertical for the teleseismic *P* phases used here. The direct *P* phase at 0 s time delay is followed by a series of peaks that represent *P*–*S* converted phases (and their multiples) generated at seismic discontinuities beneath the receiver site (Fig. 2). The direct *P* phase can be eliminated by rotating the seismograms into the ray coordinate

system (LQT) prior to deconvolution. This is helpful for identifying converted phases from shallow interfaces that would otherwise be masked by the direct *P* phase. Comparison of LQT and radial receiver functions in Schlindwein (2001) showed that the phases of interest in this study are clearly seen in the radial receiver functions which are, therefore, used in the following. The delay times of the receiver function phases are modelled by fitting traveltimes (ratio of depth and seismic velocity) to converting interfaces beneath the receiver site. The amplitudes of the phases can be used to reconstruct velocity contrasts across the converting interfaces. Information on absolute seismic velocities cannot be obtained from receiver function inversion. The presence of coherent phases in the transverse receiver functions indicates structural complexity as a plane *P* wave incident on a horizontally layered, isotropic and otherwise homogeneous medium does not generate *SH* phases (e.g. Jones & Phinney 1998).

Differences from other studies

DF and DA also use the algorithm of Ammon (1991) and comparable parameters for the calculation of receiver functions; however, the criteria they used to select earthquakes for study are different.

(i) DA use recordings from the seismometers of the permanent Icelandic network and impose selection criteria on the earthquakes that are as strict as are used here. For most stations they obtained few suitable receiver functions and, therefore, modelled single high-quality receiver functions rather than stacks. This ensures low noise levels, but the identification of relevant signals in receiver function stacks by means of narrow standard deviation bounds is somewhat easier.

(ii) DF, on the other hand, are less critical in their selection of suitable teleseismic events and use more than 40 events compared to 26 events used here. To reduce noise, they apply filters and stack normalized receiver functions over wide ranges of backazimuth and epicentral distance. For example, they include events 15–18 (Fig. 2) in the E stacks despite their different signal shapes. Complicated earth structures, such as dipping interfaces or shallow velocity contrasts that are likely to be present in Iceland, affect the amplitudes and the delay times of the phases and lead to a strong azimuthal and epicentral dependence (e.g. Cassidy 1992). Hence, stacking of normalized receiver functions over wide azimuthal and epicentral ranges results in a loss of information, which further leads to inaccurate earth models, such as overestimating velocity contrasts of deeper interfaces in the presence of shallow structures (Cassidy 1992). The receiver functions obtained by DF look qualitatively similar to those obtained here showing the main signal characteristics. However, important details such as amplitudes of the *P* phases and converted phases are difficult to compare and hence the influence of slightly different receiver functions on the resulting earth models is difficult to assess.

ICELANDIC RECEIVER FUNCTIONS

The E stacks for the radial receiver functions displayed in Fig. 3 are typical of the main features of Icelandic receiver functions. The most striking observation is the pronounced diversity of the receiver function waveforms from station to station. Comparable diagrams of receiver functions from continental areas (e.g. Kosarev *et al.* 1999) contain prominent *P–S* converted phases, which can be traced from station to station and used to generate maps of the Moho or crustal interfaces. The Icelandic receiver functions, however, generally consist of a prominent direct *P* phase and a series of low-amplitude latter phases with little consistency between the stations. The time interval within which a *P–S* converted phase from a Moho at 20–35 km would be expected is highlighted in Fig. 3. A consistent Moho *P–S* conversion cannot be identified within the marked time interval, which is characterized by different signals varying from low-amplitude phases (e.g. HOT01) to a series of more pronounced phases (e.g. HOT14, 18).

Peaks in the receiver functions at time delays >0 s need not necessarily be *P–S* conversions from deep crustal interfaces. Series of equidistant peaks with decreasing amplitudes, as observed, for example, at station HOT14 (Figs 2 and 3), may be due to reverberations at shallow depth, effectively masking potential phases from deeper interfaces. Azimuthal variation in the amplitudes of the peaks and coherent phases of the transverse receiver function (Fig. 2) provide further evidence of shallow structural complexity. In some cases, deep interfaces can only be recognized by means of their multiples (Fig. 2). For example, a *P* phase reflected at the free surface and converted to an upward travelling *S* phase at an interface in the depth range of 20–35 km arrives at 8.5–15 s time delay, whereas the direct *P–S* converted phase arrives at 2.3–4.1 s time delay (Fig. 3). In order to include these phases, the receiver functions are displayed and modelled up to 20 s time delay.

Pronounced azimuthal variation is observed for the receiver functions of stations HOT25 and 23 that are located close to active volcanoes in the Neovolcanic Zone (NVZ) (Fig. 1). Fig. 4 shows the contrasting receiver function stacks for N and WSW backazimuths at stations HOT23 and 25. The WSW stacks for HOT25 contain a series of strong phases in the transverse receiver function, which exceed the amplitudes of the radial receiver function. They are much more complicated than the N stacks for the same station. Scattering in the highly heterogeneous volcanic edifice of Askja, located to the WSW of station HOT25, may account for the unusually complicated signals of the WSW stacks. In addition, a low-velocity layer representing a magma chamber may contribute to the receiver function signal as was proposed in the receiver function study of DA for Krafla volcano. A similar model was suggested by Du & Foulger (2001) for station HOT23 near the Grimsvotn volcanic centre. I did not attempt to model the receiver functions at stations HOT23 and 25, as I felt that the data coverage was inadequate to resolve the obvious structural complexity.

An interesting feature in Fig. 3 is the consistent late arrival of the direct *P* phase of about 0.25 s for stations west of the NVZ, whereas the time delay of the direct *P* phase is zero as expected for stations east of the NVZ. The opposite observation is made for the receiver function stacks from WSW backazimuth. I showed in a separate study (Schlindwein 2001) that this phenomenon might be related to the regional dip of the lavas in the upper crust towards the centre of Iceland (e.g. Pálmason 1973). This observation indicates complicated shallow structure, which cannot be accounted for in the models. I, therefore, reduced the effect of this structure on the receiver functions by shifting the N, E and WSW receiver function stacks to match the time delay of the direct *P* phase in the stack of all receiver functions at each station. This procedure may result in inaccurate estimates of velocity contrasts (Cassidy 1992). However, considering the average shift of 0.25 s compared to the time delays of 2–4 s associated with the interesting signals, I believe that the main features of the crustal structure are still correctly reflected in the models. DA did not observe this phenomenon in their data from central Iceland (Darbyshire, personal communication, 2000), whereas DF were probably not aware of it, as they do not mention the delayed direct *P* phases.

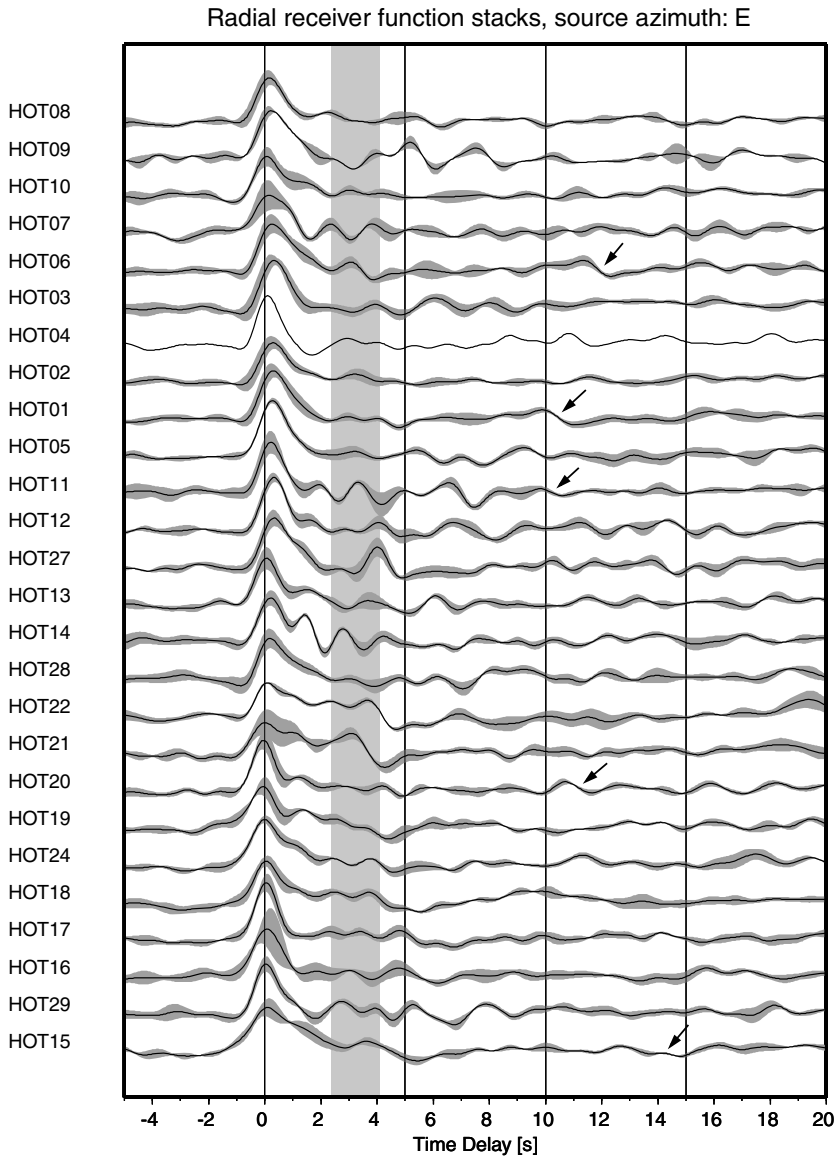

Figure 3. Overview of the radial receiver function stacks (E) and their standard deviation for all stations (except HOT23, 25, Fig. 4). The grey box marks the time delay interval where *P*–*S* conversions from a 20- to 35-km-deep interface can be expected. Arrows show examples of coherent latter phases, which need to be considered in modelling. Note that the time delay of the direct *P* phase in the E stacks is zero for HOT22-15 and non-zero for HOT08–14. The opposite applies for the WSW stack.

MODELLING RECEIVER FUNCTIONS FOR CRUSTAL STRUCTURE

The difficulties in identifying phases in the receiver functions and the spatial variability of the signals required a combined approach using inversion techniques (Ammon *et al.* 1990) and extensive forward modelling.

Method

Fig. 5 illustrates the modelling procedure. The first step, used to identify the most prominent elements of crustal structure, was to invert the stack of all receiver functions at each station. The inversion depends on a starting model, which must be sufficiently close to the true crustal structure (Ammon *et al.* 1990). I constructed a starting model (Fig. 5a) by averaging velocity–depth profiles from several seismic refraction studies (Gebrande *et al.* 1980; Bjarnason *et al.* 1993; Staples *et al.* 1997; Darbyshire *et al.* 1998) to represent the gross structure of the Icelandic crust. I incorporated a first-order Moho discontinuity at 24 km depth (Fig. 5a). The starting model was perturbed to obtain a suite of 48 models (Fig. 5a) to reduce the dependence of the inversion result on a particular starting model (Ammon *et al.* 1990). The first 20 s of the stack of all receiver functions at each station was inverted to give a 1-D velocity–depth profile for each starting model. Despite different starting models, the resulting velocity–depth profiles fitting the total stack were very similar. I, therefore, constructed the average solution and used it as first model (Fig. 5b). The next step involved careful testing of the solution, because the inversion algorithm tries to match all parts of the receiver function and cannot distinguish between noise and significant phases. Testing was also of great importance in studying the provenance of receiver function phases. As the changes in the

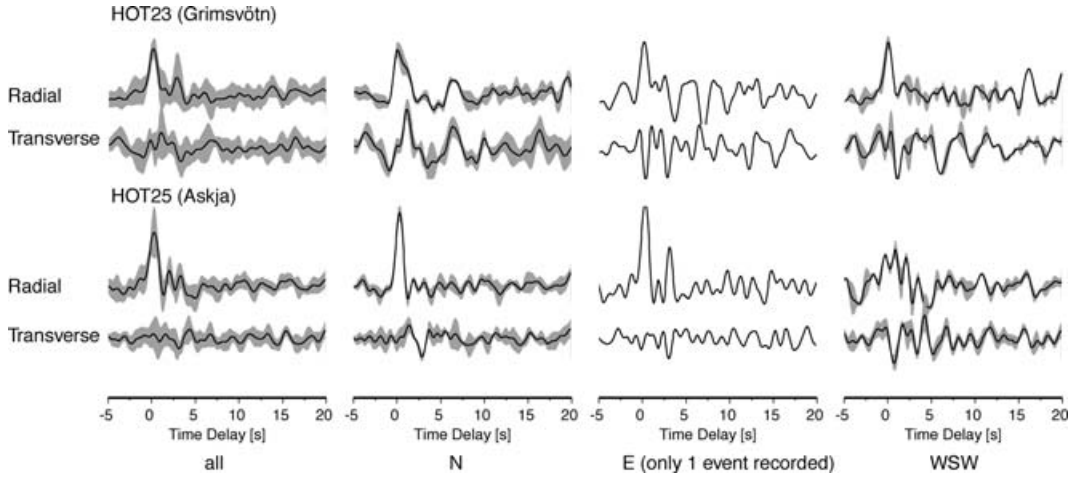

Figure 4. Receiver function stacks of stations HOT23 and HOT25 located in the NVZ close to active volcanoes. The radial receiver function signals show high-amplitude phases, which vary strongly with backazimuth. Some phases on the transverse receiver functions exceed in amplitude the corresponding phases of the radial receiver function. Note the contrasting signals of HOT25E and WSW. The ray paths of the WSW events cross Askja volcano, which lies WSW of HOT25.

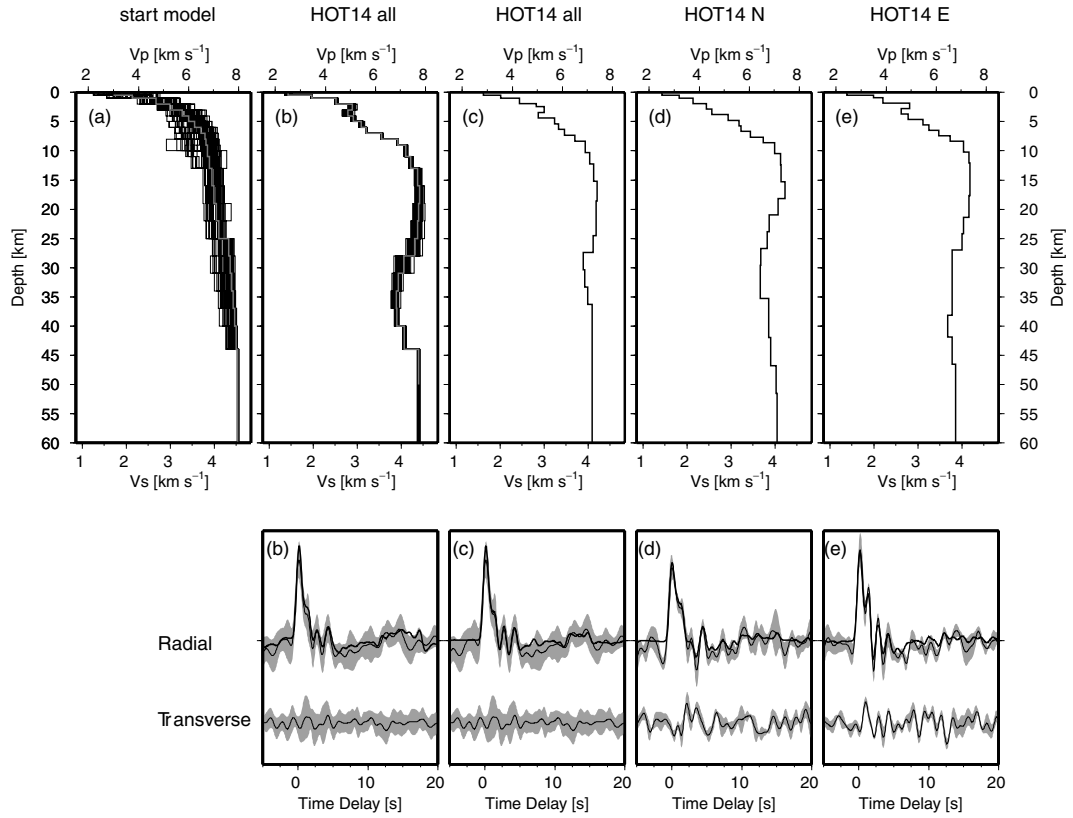

Figure 5. Modelling the radial receiver function stacks by 1-D velocity–depth profiles shown for HOT14. (a) Suite of 48 starting models for the inversion obtained by perturbing an initial model (grey) derived from previous seismic studies. These starting models are used for all stations. (b) Results of the inversion of the stack of all receiver functions at HOT14 using the starting models of (a). The results are similar and averaged (grey). The fit of the averaged model (bold line) to the receiver function stack (thin line and grey: standard deviation) is shown below. Note the misfit at 17 s time delay. The transverse receiver function is checked for large amplitude coherent phases. (c) Simplified and tested velocity–depth profile for the total stack and the corresponding fit below. (d, e) The model (c) served as starting model for the inversion and forward modelling of the more detailed N and E stacks. The WSW stack of HOT14 included receiver functions with an excessively wide range of variation and is not modelled. Final models and the comparison with the observed receiver functions are shown.

synthetic receiver function waveforms produced by a change in the 1-D velocity–depth model are difficult to anticipate, the testing phase involved several cycles of forward modelling and re-inversion of simplified or constrained models. Fig. 5(c) shows the simplified solution for the stack of all receiver functions, which matches only the most prominent phases. This model then served as starting model for the separate inversion of the N, E and WSW stacks. As the starting model is now assumed to be close to the solution, only a few

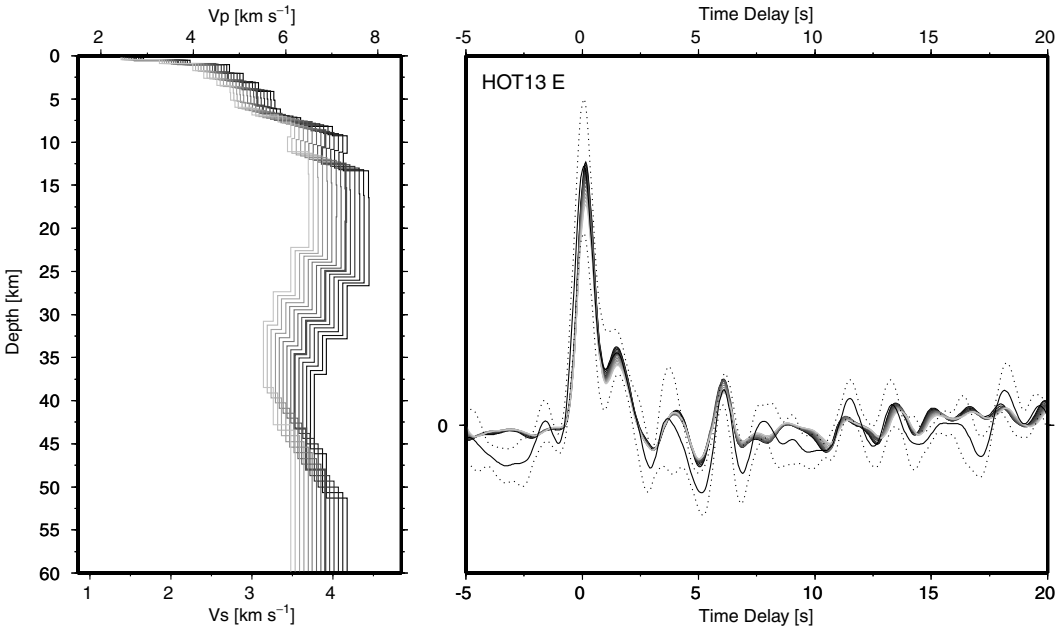

Figure 6. Velocity–depth trade-off for the receiver function models. All models fit the observed receiver function equally well (right: solid is the radial receiver function stack with dotted lines marking the standard deviation bounds). The suite of models was obtained by holding the time delay to each interface and velocity ratio across each interface constant whilst varying the absolute seismic velocity of one selected layer: the velocities and thicknesses of the other layers were adjusted accordingly. A final model (bold grey) was selected from the suite of possible solutions to match absolute seismic velocities as observed in refraction seismic studies.

alternative starting models were tested. Emphasis was again placed on intensive testing. The models for the individual stacks were further required to show similar structures and seismic velocities (Figs 5d and e). Finally, the problem of the intrinsic velocity–depth trade-off in the receiver function modelling had to be overcome by constraining absolute seismic velocities (Fig. 6). I used *P*-wave velocities from seismic studies of the upper crust (e.g. Flóvenz 1980; Flóvenz & Gunnarsson 1991) and from long-range refraction profiles, all of which show velocities of 7.0–7.4 km s^{-1} in the depth range of 10–20 km (Gebrande *et al.* 1980; Bjarnason *et al.* 1993; Staples *et al.* 1997; Darbyshire *et al.* 1998), as constraints (Fig. 6). Considering the strong lateral heterogeneity of the crust showing for example local high-velocity anomalies (e.g. Bjarnason *et al.* 1993) constraining absolute seismic velocities remained difficult. Any values given in the following for seismic velocities or interface depths, therefore, have to be considered as 'order-of-magnitude' estimates and the interpretation must focus on the existence and character of interfaces rather than on absolute values of depths and velocities.

The modelling procedure involved several parameters. The crustal structure was parametrized as a stack of layers, with constant thicknesses of 0.5 or 1 km above 10 km depth and 2 or 3 km below, bounded by a half-space below 50 km depth. The *S*-wave velocities were varied during the inversion to obtain the best fit to the observed receiver functions. *P*-wave velocities were linked by a constant Vp/Vs ratio of 1.76 (e.g. Menke *et al.* 1994) to *S*-wave velocities. Rock densities were determined from the empirical relation ρ (g cm^{-3}) = 0.77 + 0.32 Vp (km s^{-1}) (Berteussen 1977). This relation yields densities that are too low for the basaltic rocks of the upper crust in Iceland. In the *P*-velocity interval of 2.8–6.7 km s^{-1}, I, therefore, used the relation ρ (g cm^{-3}) = 3.81 − 6/Vp (km s^{-1}), proposed for basalts by Carlson & Herrick (1990).

Problems

The main source of errors in the modelling procedure is the subjective assessment of the fit of the synthetic data to the observed receiver function and the distinction between relevant and noise-related phases. A range of 1-D models can fit the receiver function almost equally well. It depends upon the interpreter which models are selected or discarded. I tried to take an unbiased approach assessing models merely by the quality of the fit. Only models with geologically unreasonable absolute seismic velocities ($Vp >$ 8.2 km s^{-1} in the uppermost 10 km of the crust) were discarded.

Fig. 7 uses examples from stations HOT21 and 14 to illustrate the difficulties encountered in modelling Icelandic receiver functions. A rapid increase in seismic velocities in the upper 8–16 km is followed by a layer of almost constant seismic velocity below. This has been observed in all seismic refraction studies and is clearly seen in this study as well. The change in seismic gradient and the structure of the upper few kilometres of the crust can account for much of the receiver function signal up to 5 s time delay (Figs 7a and d), making it difficult to correctly identify phases from deep interfaces. For stack HOT21E, the prominent trough at about 4 s seen in several Icelandic receiver functions is not matched well by the simple model (Fig. 7a). Introducing Moho-type interfaces in the typical depth range of 20–35 km depth worsened the fit (Fig. 7b). Instead, a reduction of seismic velocities at 32–37 km depth (Fig. 7c) produced the best fit to the trough and a multiple at 15 s, giving some confidence in this model. The trough at 9 s is not modelled since a large coherent transverse phase at 9.5 s is present, indicating lateral inhomogeneity. Figs 7(d)–(f) show the same testing procedure for stack HOT14E. The upper crust contains a velocity inversion which, together with the change in seismic gradient, accounts for the first 5 s of the receiver function signal (Fig. 7d). Phases from deeper interfaces are masked by a suite of shallow reverberations. The

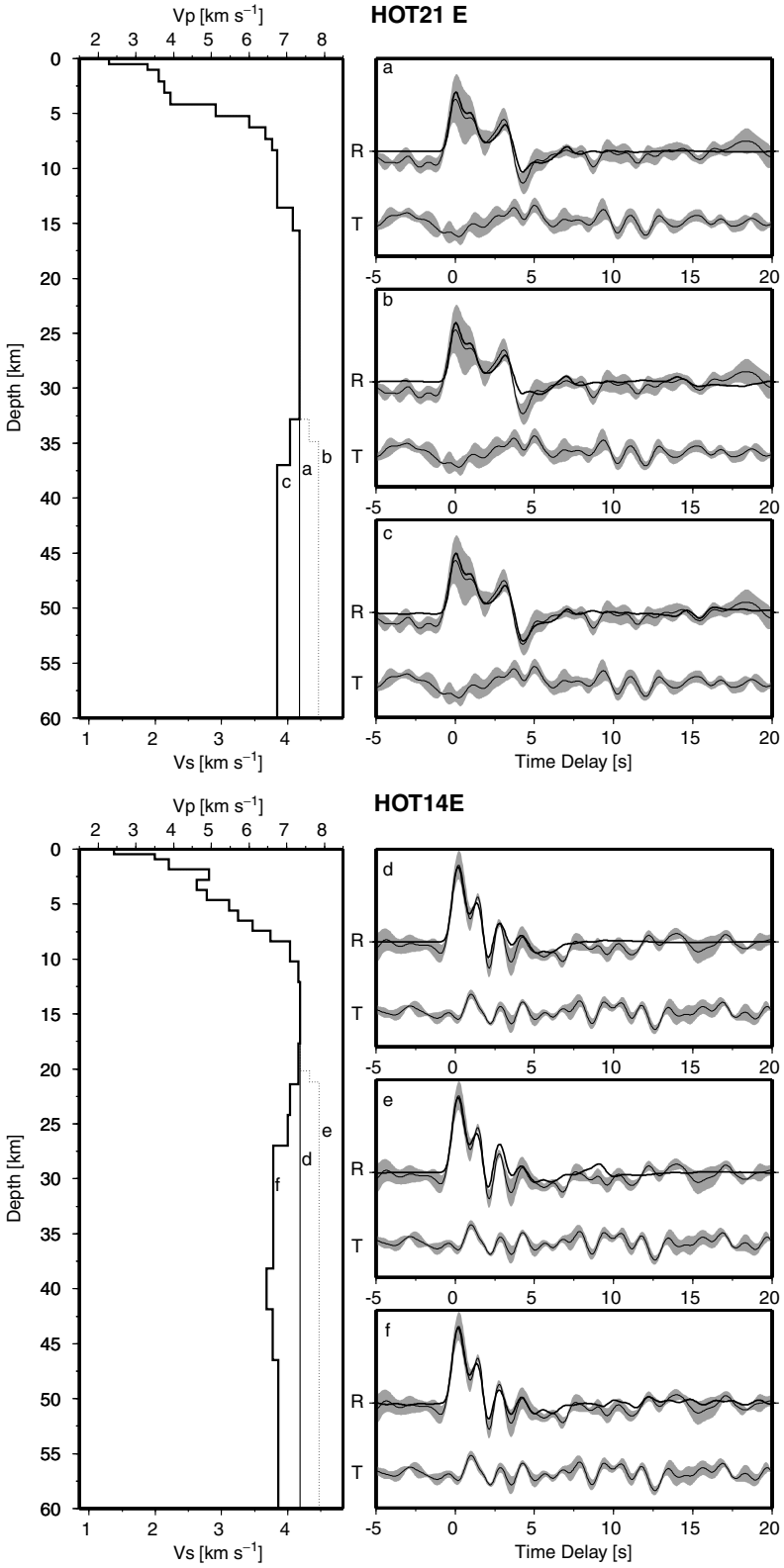

Figure 7. Analysis of receiver function signals at the example stations HOT21E and HOT14E. Left: various velocity–depth models a-f. Right: the synthetic receiver functions (bold line) of models a-f are compared to the observed radial (R) and transverse (T) receiver function stacks (thin line; grey shading: standard deviation). HOT21E: (a) The upper crustal structure produces most of the signal during the first 4 s. The steep flank at 3–4 s is not adequately matched. (b) A Moho at 32 km depth clearly deteriorates the fit. (c) A velocity inversion at 32–37 km depth produces the best fit including a multiple phase at 15 s. HOT14E: (d) The velocity inversion and the change in seismic gradient at 11 km depth account for most of the first 5 s of the receiver function. (e) A Moho at 20 km depth slightly deteriorates the fit to the peak and trough around 3 s. (f) The best fit to the trough at 3 s is achieved by a small velocity decrease. A decision between models (d)-(f) is difficult because of a large transverse phase at 3 s.

corresponding phases of the transverse receiver function almost reach the amplitudes of the radial, indicating deviations from 1-D structure. Therefore, it is difficult to judge whether the slightly better fit to the peak and trough around 3 s time delay offered by the model (Fig. 7f), which includes a velocity inversion at depth, is sufficiently significant to exclude the model (Fig. 7e), which contains a Moho. Whereas a model with a velocity inversion could be selected with some confidence for HOT21E, this is more difficult for HOT14E. Similar tests were performed during the modelling procedure for all stations.

Another problem concerns the large azimuthal variability of the receiver functions. I did not attempt to model any stacks that included receiver functions with very different waveforms. Neither an average receiver function nor an arbitrarily chosen single receiver function is likely to represent the true crustal structure at such a location. Stations HOT17 and 19, for example, showed very little signal coherency within the stacks and between the stacks and were, therefore, excluded. Figs 8–10 show the velocity–depth profiles and the fit to the best-constrained receiver function stacks, which is in most cases the E stack. The velocity–depth profiles for other reliable receiver function stacks are included for comparison. HOT15, for example, shows very similar results for all azimuths whereas HOT24 (Fig. 10) is an example of the pronounced azimuthal diversity indicating very heterogeneous crustal structure.

The average *S*-wave velocity in the crust is roughly 3.7 km s^{-1} corresponding to a wavelength of 7 km for a maximum signal frequency of about 0.5 Hz. The width of the first Fresnel zone at a depth of 25 km is then about 27 km, and the vertical resolution of a quarter wavelength amounts to 1.75 km. Taking 2.5 km s^{-1} as representative *S*-wave velocity of the upper crust, the vertical resolution is 1.25 km and the width of the Fresnel zone is 12 at 6 km depth. Hence, crustal properties are sampled along a tube surrounding the ray narrowing towards the station. Due to steep but non-vertical ray incidence, different areas around a station are sampled by the stacks. The 1-D velocity–depth models, therefore, still represent 1-D point measurements which, considering the heterogeneity of the Icelandic crust, should not be extrapolated. In contrast, the ray paths of refraction studies in contrast travel subhorizontally through the crust and, therefore, sample crustal structure over a wider range along the profile; details of structure are resolved by dense station spacing. These intrinsic differences between receiver functions and refraction data have to be considered when comparing in detail the results.

Differences from other studies

(i) DA used a very similar modelling approach to that presented here including forward modelling and testing, which is well suited for the specific problem of Icelandic receiver functions. However, I gained the impression that they may partly have underestimated the difficulties of phase identification with reverberations from the pronounced shallow structure masking *P–S* conversions from a potential Moho. They attributed a phase at 2 s time delay to a Moho at 16 km depth and, at a different place, a phase at 4 s to a velocity step at 4 km depth without distinguishing between reverberations and *P–S* converted phases. Furthermore, their selection of final models sometimes appears to be influenced by their results from a seismic refraction study (Darbyshire *et al.* 1998). 1-D velocity–depth models showing no Moho were discarded (station GRI), a sharp Moho discontinuity was introduced where the inversion suggested a velocity gradient (station GRA) or models in agreement with the seismic refraction results were preferred over alternatives despite a less convincing fit (station SKR).

(ii) DF perform a joint inversion of surface wave dispersion curves and receiver functions. In their earlier studies, they select those receiver function models from a suite of inversions that also explain the surface wave data to some extent. Du *et al.* (2002) use an improved approach, where a starting model for the receiver function inversion is obtained by inversion of the surface wave dispersion curves. Three to five control points of the resulting velocity depth profiles were held fixed during the subsequent receiver function inversion. This method of constraining absolute velocities is superior to the qualitative scheme used here and by DA. However, it assumes that medium properties do not vary much from average, since surface waves and receiver functions do not sample the same crustal regions. This assumption may not be valid everywhere in Iceland bearing in mind the pronounced heterogeneity of the crust. It implies the risk of a detailed but incorrect constraint of absolute velocities.

(iii) DF interpret averaged and simplified final models derived from the different stacks at a station without performing forward modelling. Hence, distinguishing between noise and signal phases and, thus, true and apparent structure is difficult. For example, a phase at 3 s time delay is considered a *P–S* conversion from the Moho at 23–27 km depth, but the model for station HOT06N showed a Moho and no phase at 3 s and vice versa for HOT08SW (Du & Foulger 1999). In addition, in the simplified models, structure required to fit the receiver functions is sometimes discarded, whereas features similar to a Moho are preferentially kept, although forward modelling would show that they do not contribute to the relevant receiver function signal. This is difficult for the reader to judge as DF do not show how well their simplified final models fit the receiver functions. For example, more than 15 of their inverted models contain a large *S*-wave velocity inversion of up to 0.8 km s^{-1} in the uppermost 5 km of the crust. This extreme structure is likely to contribute to the shape of the *P* peak and produce a suite of reverberations at larger time delays. None of the simplified models contains this structure and DF do not discuss its origin. It might be an artefact of the inversion routine rather than real structure. As I did not derive this sort of structure for most stations, the reason may lie in differences between our approaches: DF use the unmodified density–velocity relationship of Berteussen (1977) and hence excessively low densities in the shallow crust. DF were not aware of the delays of the *P* peak as described before and the inversion tries to model 1-D shallow structure even though the observations are due to 2-D or 3-D effects.

Results

Figs 8–11 show the resulting 1-D velocity–depth profiles for each station. The receiver function models have been grouped according to similarities in the seismic structure rather than, for example, crustal age.

Western Fjords (HOT06–10)

Seismic velocities increase rapidly in the upper 6–10 km and are underlain by a layer of almost constant velocities (Fig. 8). Stations HOT06 and HOT07 show a velocity increase at 27–32 km depth and some indication of a small velocity decrease below this. Du & Foulger (1999) present a similar model for both stations. The results of both studies for HOT08 are comparable, but no significant impedance contrast is found at this station and data quality was poor. I obtained results for stations HOT09 and HOT10 that differed from those of Du & Foulger (1999). Whereas Du & Foulger (1999) found

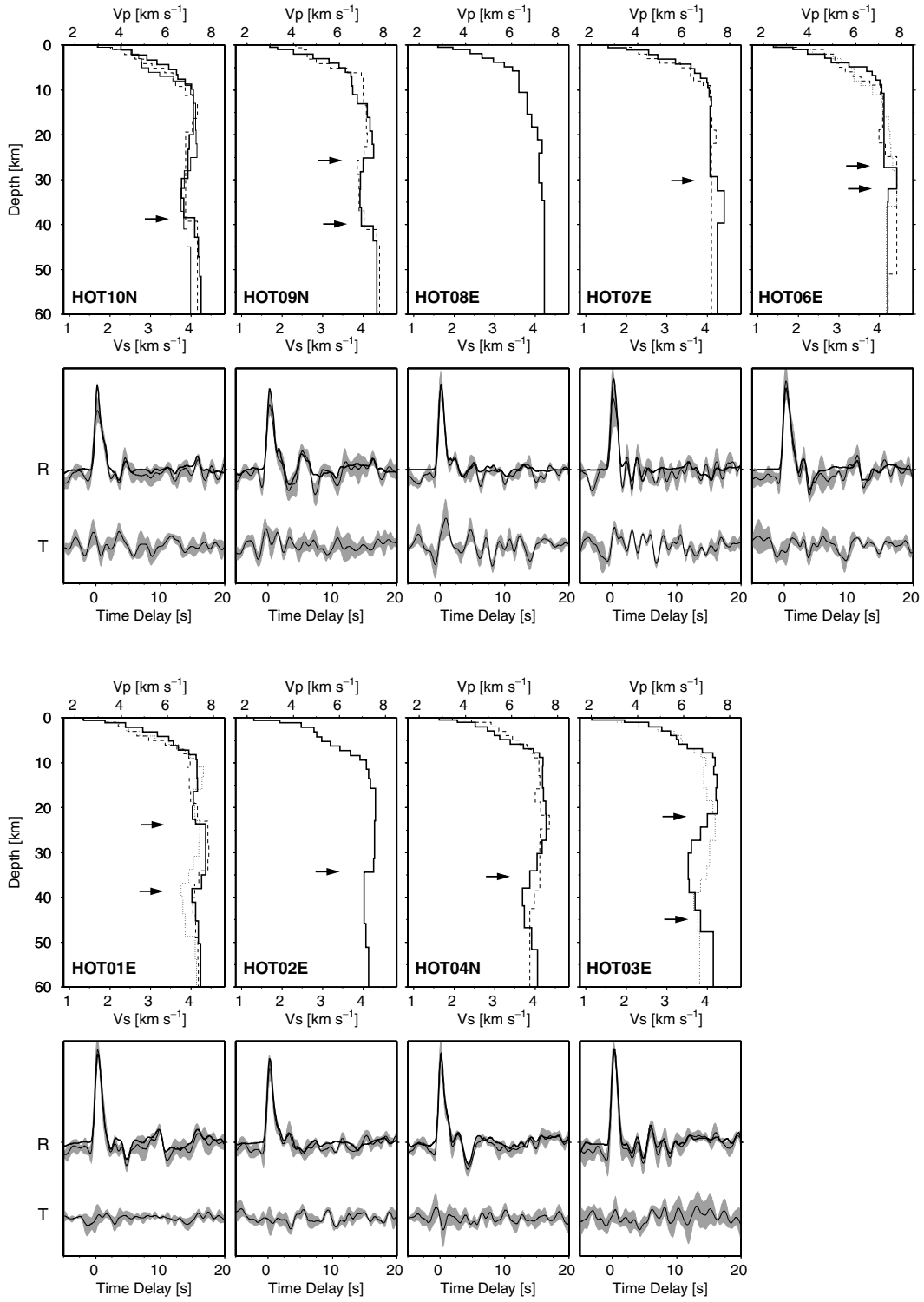

Figure 8. Velocity–depth models of the crust beneath receiver sites in the Western Fjords and West Iceland. The bold line shows the best-defined model for the indicated stack, usually E. Models for other stacks are shown by dotted (N), dashed (WSW) or thin (E) lines. The synthetic receiver functions of the best-defined models (bold line) are compared to the observed radial (R) and transverse (T) receiver function stacks (thin line; grey: standard deviation). The change in seismic gradient at 6–14 km depth is seen in all receiver function models in Iceland. Arrows indicate additional well-constrained interfaces.

smoothly increasing velocities with depth free of discontinuities, a positive impedance contrast at 38–40 km depth was required here to match a phase at 4–5 s time delay, which is despite higher levels of pre-signal noise also present in their receiver functions. It is difficult to decide which of the models reflects true structure as Du & Foulger (1999) do not show how well their models fit the receiver functions and they limited their modelling to a maximum of 40 km depth. This may not be sufficiently deep forcing the inversion to match

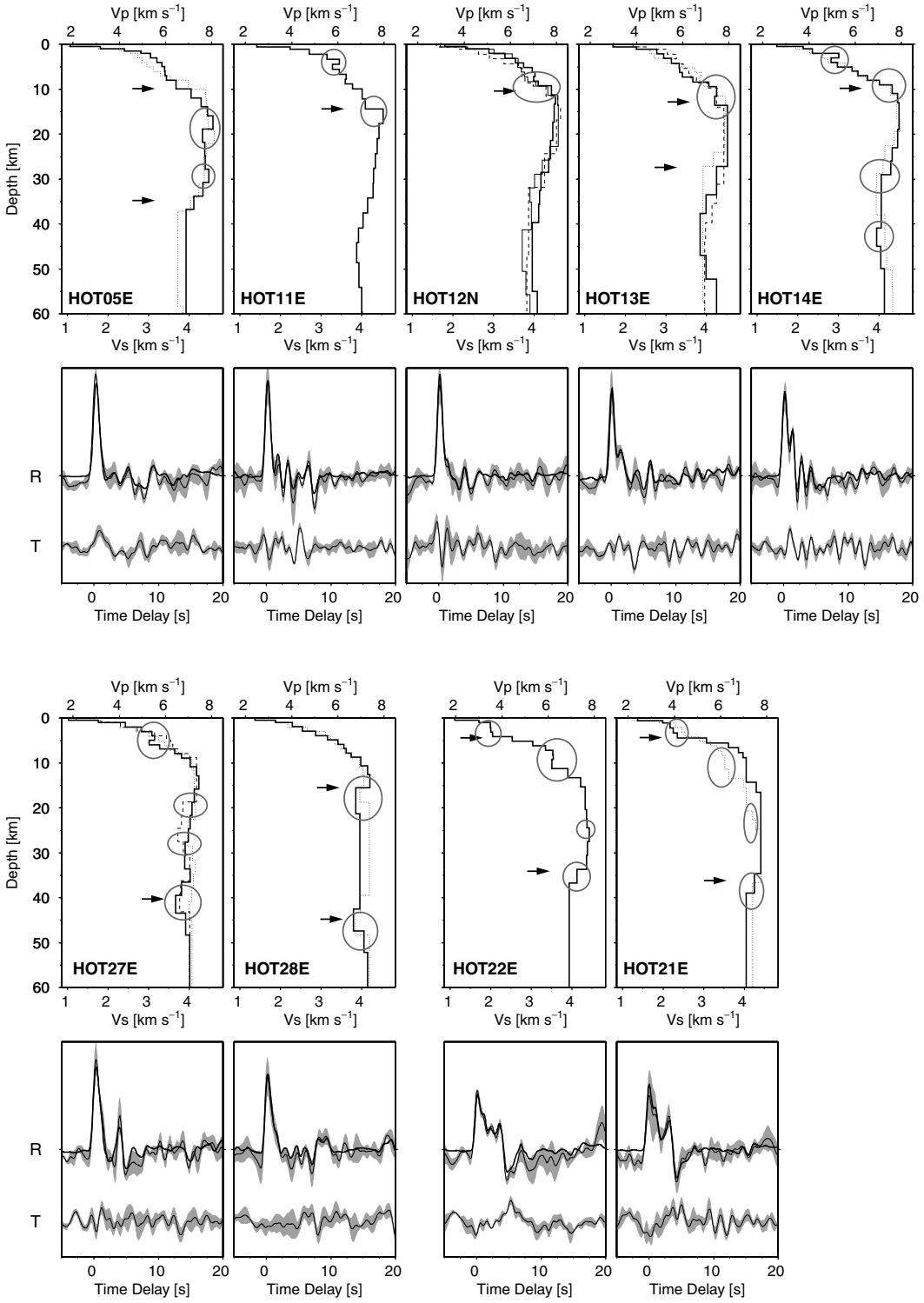

Figure 9. Velocity–depth models of the crust beneath receiver sites in central northern Iceland and South Iceland. Circles mark discontinuities also identified by Du & Foulger (2001) and Du *et al.* (2002). See Fig. 8 for legend.

the observed phases with reverberations within the shallower structure. Considering the differences in the methodological approach of these studies, the results for stations HOT06–08 seem to be robust, whereas no conclusive models could be obtained for the receiver functions of HOT09 and 10.

West Iceland and Snæfellsnes (HOT01–04)

The same pattern of seismic velocities increasing rapidly to about 8 km depth underlain by almost constant velocities is observed for stations HOT01–04 (Fig. 8). HOT01 shows a discontinuity at

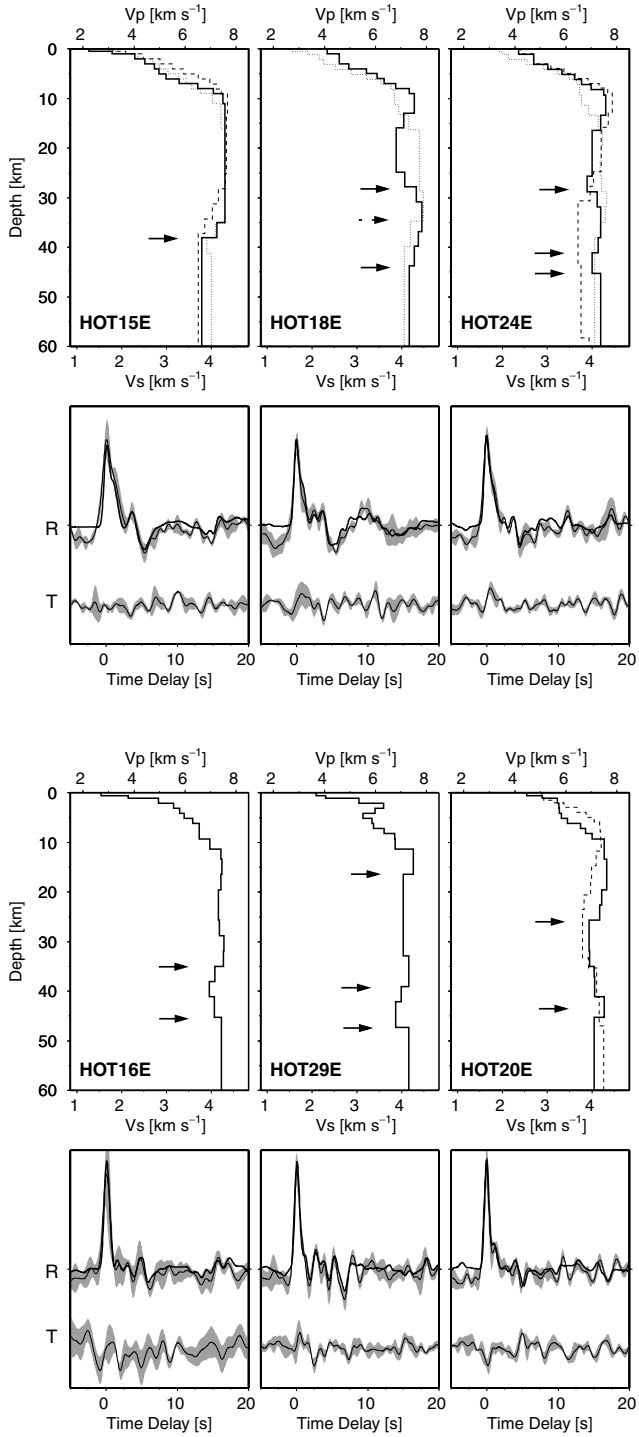

Figure 10. Velocity–depth models of the crust beneath receiver sites in East Iceland. See Fig. 8 for legend.

22–24 km depth and a tendency to reduced velocities at 33–40 km depth. Du *et al.* (2002) obtained similar receiver functions and models for all three stacks of HOT01; however, they do not include a velocity decrease at 33–40 km depth in their final models although it improves the fit to the negative phase at 4 s time delay. Equivalent models are also proposed by DA for the nearby station ASB/BORG with a pronounced velocity discontinuity at 25 km depth. Some of their model families also show a weak velocity inversion below, which they did not consider relevant.

The receiver functions at HOT02 and HOT04 display well constrained negative phases at about 4 s time delay modelled by analogy to station HOT01 by decreasing velocities at about 35 km depth. The models of Du *et al.* (2002) differ showing increasing velocities at 25 and 40 km depth. Their original models, but not the simplified final models, contain a pronounced velocity inversion in the upper 5 km of the crust (see discussion above), which may account for the different styles of the models. As no forward modelling is performed by Du *et al.* (2002) to check the robustness of the velocity discontinuities, and the fit of the final model is not shown, it is again difficult to decide between the conflicting results of the two studies.

Stacks HOT03N and HOT04WSW sample the area north of Snæfellsnes and show a velocity increase at about 20 km depth and a decrease at about 40 km depth, whereas a pronounced velocity inversion at 25–40 km depth is seen at HOT03E underneath the Snæfellsnes off-rift flank zone (Fig. 1). Du *et al.* (2002) present broadly similar models, however, the velocity inversion is less pronounced and limited to the depth range between 30 and 40 km.

Central northern Iceland (HOT05, 11–14, 27, 28)

A complicated upper crustal structure is typical of this area west of the NVZ. Stations HOT05, 11–14 are located within or close to extinct central volcanoes (Jóhannesson & Sæmundsson 1998) that are known to exhibit unusual seismic characteristics such as anomalously high seismic velocities (e.g. Flóvenz 1980; Brandsdóttir *et al.* 1997). Here, shallow velocity inversions are seen at several stations such as HOT11, 14 and 27 in this study (Fig. 9) and in Du *et al.* (2002) and Du & Foulger (2001). The gradient layer in the upper 10–14 km and the very pronounced change to constant or decreasing velocities below produces much of the receiver function signal, which often includes reverberations from the gradient layer. Comparison of the models reported here with those of Du *et al.* (2002) and Du & Foulger (2001) nicely illustrates that the limited ability of the receiver function method to constrain the long-wavelength shape of the velocity–depth profiles and deeper impedance contrasts. I marked with circles discontinuities in the models of Fig. 9, which are also found by Du *et al.* (2002) and Du & Foulger (2001). For stations HOT05 and 11–13 the shape of the velocity–depth profiles differs markedly in our studies illustrating that the receiver functions can define only the common velocity discontinuities in the upper crust but cannot resolve the deeper structure. The approach of Du *et al.* (2002) including surface wave information is better suited to recover the long-wavelength shape of the velocity–depth profiles. Thus their results may be deemed more reliable for these stations. However, the lack of any forward modelling may limit the usefulness of their results. This becomes evident, for example, for station HOT27. Stations HOT27, 28 and 14 all yielded very similar earth models in our studies including a deep velocity inversion between 40 and 50 km depth as shown by the circles in Fig. 9. For HOT27, the simplified final model of Du & Foulger (2001) no longer includes the velocity inversion at 5 km depth and the velocity reductions at 20 km and 40 km depth, but it enhances the discontinuity at 30 km depth, which is seen here only weakly for the WSW and N stacks and is not well constrained by the receiver functions. Hence, the final model of Du & Foulger (2001) for HOT27 showing a Moho at 30 km depth and no other discontinuities is unlikely to account for the observed receiver function.

South Iceland (HOT21, 22)

Stations HOT21 and 22 show receiver function signals that are distinctly different from those of the other stations (Figs 3 and 9). The *P* peak is followed by a broad plateau of high amplitudes, cut off by a steep flank and trough at 3–4 s. The shape of the *P* peak was difficult to define for station HOT21E as the size of the *P* peak and the trough at about 2 s varied even for high-quality events as shown by the large standard deviation bounds of the stack. Due to different selection criteria, the stack of Du & Foulger (2001) showed a deeper trough at 2 s than Fig. 9. The steep flank at 3 s is well constrained and observed for all azimuths on both stations and in both studies. The broad plateau results from an unusual upper crustal structure with a surface layer of about 5 km thickness and low velocities. Below, velocities increase rapidly and constant velocities are reached at 14 km depth. The results of Du *et al.* (2002) for HOT22 and of Du & Foulger (2001) for HOT21N and E show the same upper crustal structure as is observed here. The velocity increase at 5 km depth for HOT21E is smaller in their model, more like that of my model for HOT21N. This may indicate, that their stacked receiver function waveform HOT21E is more representative than the one shown here.

Refraction seismic studies (e.g. Flóvenz 1980; Flóvenz & Gunnarsson 1991) have demonstrated the presence of anomalously thick upper crust in southern Iceland. As HOT22 lies within this area of thick upper crust, but HOT21 just off its eastern margin, this correlation of refraction seismic and receiver function results is somewhat speculative.

The steep flank and the trough in the receiver function signal required a velocity inversion at about 34–36 km depth for both stations in my models. Decreasing velocities at 30–35 km depth are also discernible in the models of Du & Foulger (2001) and Du *et al.* (2002); however, in their final models, they keep velocity increases at about 25 km depth, which are only weakly developed in my models HOT22E and HOT21N, and a large velocity increase at 45 km depth for HOT22, which is not seen here. Hence, the comparison of the two studies indicates that the 1-D crustal structure in south Iceland qualitatively looks like the model HOT22E with well-defined velocity contrasts in the upper crust and further impedance contrasts at about 25 and 35 km depth whose magnitude can not be defined reliably.

East Iceland (HOT15–20, 24, 29)

East Iceland shows receiver functions with weak and incoherent phases. The best-constrained stacks were selected for modelling and are shown in Figs 10 and 11. Station HOT29 is located in the area of a fossil dyke swarm (as are the excluded stations HOT17 and 19) (Jóhannesson & Sæmundsson 1998). The complicated receiver function and the resulting velocity–depth profile including a shallow velocity inversion may result from the effects of local dykes. Apart from stations HOT15 and 16, the surface velocities in the east are higher than elsewhere. Refraction seismic studies show comparable surface velocities for this area (Darbyshire *et al.* 1998). The change in seismic gradient is located at about 10 km depth in East Iceland.

The deep structure of East Iceland is complicated. Station HOT15, and also the stacks HOT18N and 24WSW (Fig. 10), point to a marked velocity decrease at about 35 km depth. Towards the east, stacks HOT18E, 24E, 29, 16 and 20 indicate a zone of structural complexity in the depth range of 29–45 km with frequent velocity changes. These deep discontinuities cannot be traced from station to station and differ depending on the stack azimuth, suggesting strong structural heterogeneity in this area.

Comparison with the independent results of Du *et al.* (2002) and Du & Foulger (2001) helps to identify which aspects of the structure have been reliably determined. Many of their models include shallow velocity inversions (see discussion above) that are not required by this study, for example, in the models of HOT24N and HOT18E, N. However, the most prominent deep velocity contrasts are similar for these stations: The models of Du *et al.* (2002) for stacks HOT18N, ESE[1]) also show increasing velocities at about 28 km depth and for HOT18N decreasing velocities at about 35 km depth. The clear velocity increase at station HOT24E at 30 km depth is recovered by both studies, however, a small range of decreasing velocities is found in this study at 40–44 km depth and at about 36–40 km depth by Du & Foulger (2001). In that article they show how the inverted (but not the simplified) models of the individual stacks fit the observed receiver function. For HOT24E, it is evident that the synthetic receiver function obtained from my models fits the observed signal better than the results of Du & Foulger (2001), especially for the multiple at about 16 s, giving greater confidence in the depth estimate of the velocity inversion proposed here.

The results for stations HOT15, 16, 20 and 29 differ between the two studies. For the latter three stations, azimuthal variability of the very complex signals was large and hardly any common impedance contrasts are found apart from similar upper crustal structure. The receiver functions for HOT15 show a more uniform shape for all stacks, which clearly differs from that of stations HOT16, 20 and 29. Correspondingly, the model for HOT15 in my study differs from that of stations 16 and 29 and looks more like HOT18N. Du *et al.* (2002), however, propose a common final model for stations HOT15, 16 and 29 with an *S*-wave velocity increase of 0.6 km s^{-1} over the depth range 30–50 km. Such a small gradient does not produce a detectable converted phase in the receiver functions. Rather, it results from the constraint imposed by the surface wave data, which indicate increasing velocities below roughly 20–30 km depth. Hence, the upper boundary of this gradient layer is not well constrained by either data set. In addition, considering the different shapes of the receiver function signals for HOT15, 16 and 29, it is evident that one common simplified model can not satisfy the observations. On the other hand, the velocity decrease at about 35 km depth in my model for HOT15, which produces the steep flank of the receiver function at 4 s time delay and the multiple at 16 s, seems to contradict the surface wave data, which indicate increasing velocities at 30 and 40 km depth and constant velocities in between. A joint inversion to better constrain absolute velocities combined with forward modelling of the receiver functions is needed to see how both data sets can be satisfied by one model.

INTERPRETATION AND DISCUSSION

Difficulties

The above description of the 1-D earth models (Figs 8–10) obtained from receiver function inversion illustrates the great diversity of the

[1]The results of HOT18E of this paper have to be compared with the results of HOT18ESE of Du *et al.* (2002) (their Figs 11–13). The results are based on the same receiver functions (*cf.* Table 1 and their Fig. 12) with east–northeasterly backazimuth. The term HOT18ESE in Du *et al.* (2002) is misleading and should read HOT18ENE.

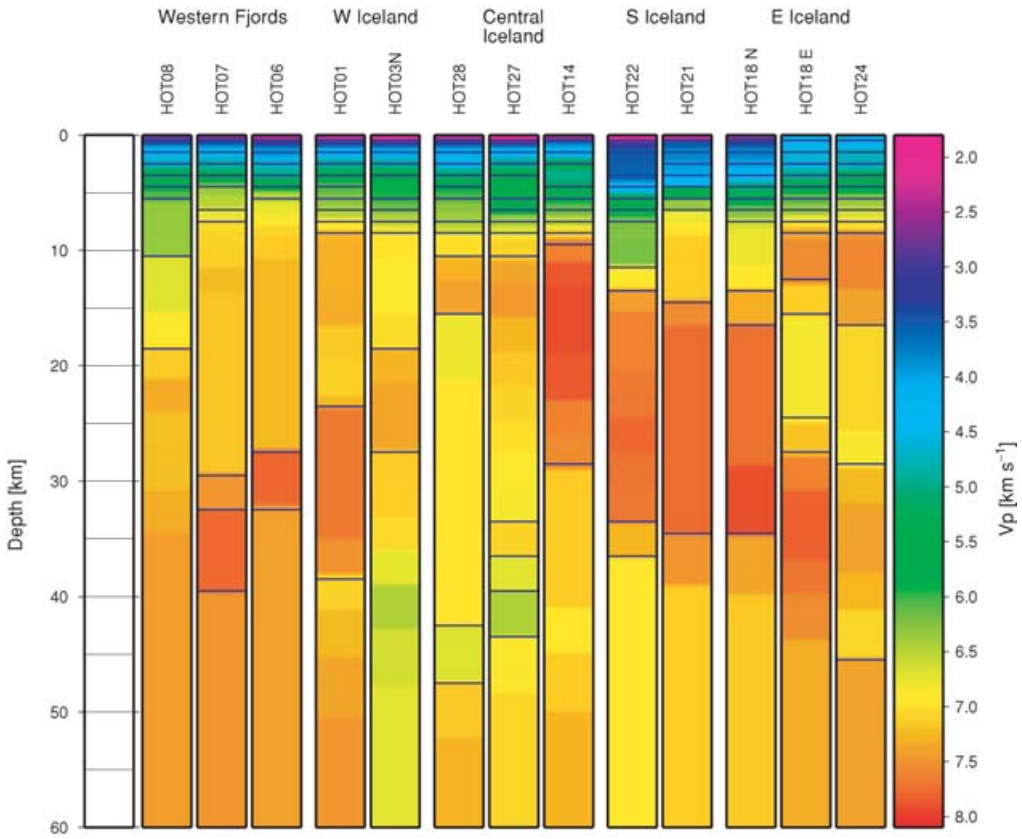

Figure 11. Crustal structure of Iceland derived from receiver function modelling. Only models similar to the corresponding models of DF are shown. Note that absolute seismic velocities and deep structures are not well defined. Layer boundaries with more than 3 per cent relative velocity change are highlighted in blue. Note the area of reduced seismic velocities at about 40 km depth beneath stations HOT01-18N.

results. A common feature is the rapid increase of seismic velocities in the upper crust followed by almost constant velocities. This change in gradient can be used as a measure of the thickness of the upper crust. The upper crustal thicknesses agree qualitatively with those measured by seismic refraction profiles (e.g. Darbyshire *et al.* 1998; Staples *et al.* 1997; Menke *et al.* 1998; Bjarnason *et al.* 1993; Flóvenz 1980) as shown for example by DF. I concentrate the interpretation here on the crust–mantle transition. Finding a criterion to define the position of the Moho is difficult as it is not connected with any distinctive common feature such as a velocity discontinuity of a certain minimum size. DA, therefore, define the Moho where mantle velocities of $Vs = 4.4$–4.5 km s^{-1} are reached. The character of the velocity contrast connected to the thus-defined Moho varies from a pronounced first-order velocity discontinuity with an increase in *S*-wave velocity from 3.5 km s^{-1} to 4.5 km s^{-1} to a 10 km thick gradient zone with a small discontinuity at its base. These differences in the character of the crust–mantle transition are difficult to account for in any interpretation of the variations of crustal thickness.

DF derive the depth to the Moho using the $Vp = 7.2$ km s^{-1} ($Vs = 4.1$ km s^{-1}) horizon in the inverted but not simplified models (Du & Foulger 1999, 2001) and in the simplified models (Du *et al.* 2002). As no forward modelling is performed to check for relevant structure, both approaches involve the risk of an ill positioning of the Moho. The original inverted models may contain unnecessary structure resulting from inversion of noise-contaminated receiver functions. Hence, small changes in the shape of the velocity–depth profiles, especially in the absence of major velocity discontinuities, may lead to a considerably different position of the Moho horizon without deteriorating the fit to the observed receiver function signal. As some of their simplified models retain unnecessary structure, the exact position of velocity horizons remains speculative. Hence, quantitative estimates of the Moho depth from Icelandic receiver functions have to be used with great care.

I make use of the independent results of DF to derive a qualitative interpretation of the earth models. Fig. 11 shows the models, which display largely similar structures in both studies. As these models are tested in this study for their robustness by forward modelling and are similar to the models constrained by surface wave information by DF, they can be considered more reliable than the results of any single study. Nevertheless, the interpretation of the common models has to remain qualitative, focusing on the existence or non-existence of velocity contrasts rather than on their accurate position and size. For this qualitative interpretation, subjectivity in the assessment of the reliability of receiver functions and models and differences in methodological approach seem to play no major role. This further implies that conflicting models in our studies indicate structural complexity, which is poorly defined by receiver functions and 1-D models rather than a single method being ill suited (although each of the approaches has its advantages and shortcomings as discussed before).

Moho

The following statements about the crust–mantle transition in Iceland can be made on the basis of the receiver functions:

(1) A continuous classical Moho with a large velocity increase is not present in Iceland. The receiver function method would be able to detect such a discontinuity. This is demonstrated for example by station HOT01, where all receiver function studies found a velocity discontinuity at about 22–24 km depth in agreement with the nearby refraction profile (Bjarnason *et al.* 1993). Complex upper crustal structure could eventually mask even a prominent Moho, as demonstrated for station HOT14 in Fig. 7. However, as small and gradational velocity increases mark the Moho at other places, for example HOT03N, a classical Moho everywhere underneath Iceland, which is merely masked in places appears unlikely.

Recent gravity studies (Kaban *et al.* 2002; Gudmundsson 2003) offer further support for a small impedance contrast across the Moho. Both studies suggest that densities in seismic layer 4 defined by *P*-wave velocities of 7.0-7.2 km s^{-1} are higher than normal and higher than in the lower crust of the adjacent oceanic areas. This may explain why the seismic manifestation of the Moho becomes more pronounced towards the Reykjanes Ridge, where Weir *et al.* (2001) identified clear PmP reflections. Kaban *et al.* (2002) thus interpreted seismic layer 4 in Iceland as a transitional layer between crust and mantle with alternating mafic and ultramafic material, whereas Gudmundsson (2003) suggested that lower crustal material enriched in olivine and iron and phase transitions in the lower crust may result in high densities without invoking compositional changes.

(2) The character of the crust–mantle transition is highly variable across Iceland. It may have the more classical appearance such as at stations HOT01 or HOT06, it may be almost absent as at HOT08E, or it may be characterized by a thick gradient zone such as at HOT18. This variability is also emphasized by the independent studies of DA and DF. For some stations, such as HOT21 and 22, the position of the potential Moho is not obvious from one study alone. Du *et al.* (2002) and Du & Foulger (2001) show somewhat larger velocity increases at 25 km depth than seen here for HOT22E. Darbyshire *et al.* (2000b) obtained a crustal thickness of 25 km for this area from gravity modelling suggesting that this small velocity increase may signal the crust–mantle transition. A similar situation exists for stack HOT3N with a small velocity increase at 20 km depth, which would again fit the Moho depth estimates for this area (Darbyshire *et al.* 2000b). The variability in the character of the seismic Moho does not contradict the seismic refraction results. The presence of PmP phases on the seismic refraction profiles (Bjarnason *et al.* 1993; Staples *et al.* 1997; Darbyshire *et al.* 1998) is evident, but the phases are typically observed over small offset ranges. Ray tracing shows that the areas where the Moho boundary is actually constrained by seismic rays are not interconnected and extend to a maximum lateral dimension of 20–30 km. The variability of the receiver function models, the possible reason for the high densities of seismic layer 4—be it of compositional or chemical nature (Kaban *et al.* 2002; Gudmundsson 2003)—and the history of rift jumps in Iceland (Sæmundsson 1979) all point to a highly heterogeneous lower crust and hence support a regionally variable style of the crust–mantle transition.

Upper mantle

The receiver function models for HOT01 show a velocity decrease in the upper mantle about 15 km below the Moho. This velocity inversion is also present under the thick crust of central Iceland for stations HOT27 and 28. The low-velocity zone is also seen in my models for South Iceland (HOT21, 22). Towards the northwest Fjords the velocity decrease becomes less pronounced for stations HOT06 and HOT07 and is absent for HOT08. Towards the east, the margin of the low-velocity zone may be present at the eastern margin of the NVZ. Stations 18N and 24WSW, sampling just east of the rift, show a well-constrained velocity reduction at depth not seen in comparable clarity for HOT18E and 24E and in my models for the eastern stations HOT16, 29 and 20. While the upper boundary of the velocity inversion varies across central Iceland from about 35–42 km depth, minimum velocities are reached mostly at about 40–45 km depth.

Indications of a velocity inversion in the upper mantle are also present in the studies of DA and DF, but these studies are mainly concerned with the character of the crust and the Moho and do not specifically analyse this feature. Taking all receiver function studies together, the presence of this velocity inversion has to remain speculative and should be examined in more detail. However, the existence of a low-velocity zone in the upper mantle does not seem unlikely in the light of other studies:

(1) Wolfe *et al.* (1997) calculated station terms for their tomographic model of the mantle beneath Iceland. These station terms represent vertical *S*-wave traveltimes for the upper 100 km beneath Iceland and are a measure of integrated differences in the crustal and mantle structure beneath the stations. These delays in *S*-wave traveltime in the upper 100 km occur in the roughly the same area as the velocity reduction in the receiver function models. Significant advances of *S*-wave arrivals are seen for East Iceland. The crust in East Iceland is thought to be thicker than in northern Iceland (e.g. Darbyshire *et al.* 1998), which as long as the *S*-wave velocity is similar would have the opposite effect on the traveltimes as is observed. The origin for the *S*-wave delays must, therefore, be sought in the upper mantle, supporting the identification of the low-velocity zone in the receiver function models. A prominent gradient from *S*-wave delays to *S*-wave advances is seen at the eastern margin of the NVZ. This might agree with the proposed margin of the low-velocity zone in this area.

(2) Bjarnason (1999) inverted surface wave dispersion curves for the crustal and mantle structure beneath Iceland. He found mantle material with *S*-wave velocities of 4.3–4.5 km s^{-1} at 45–80 km depth beneath East Iceland, which he interprets as lithospheric mantle. Reduced seismic velocities below 80–100 km are considered to represent the asthenosphere. In contrast, dispersion curves for a path, which runs parallel to the rift zone in the area of HOT15, 18N, 21 and 22, indicate that a comparable lid of lithospheric mantle is less than 15 km thick or even absent. In this area, Bjarnason (1999) observed a velocity inversion to *S*-wave velocities of 3.7–3.9 km s^{-1} at about 40–50 km depth, which he inferred to indicate a considerably shallower asthenosphere than under East Iceland. This would broadly agree with the receiver function results.

(3) Finally, Kaban *et al.* (2002) derived from their gravity models the position of the 1200 °C isotherm below which partial melting is thought possible. The presence of partial melt would drastically reduce the *S*-wave velocity and increase the Vp/Vs ratio. This would result in an impedance contrast observable by the receiver functions. The simple 1-D modelling of receiver functions presented so far assumed a constant Vp/Vs ratio such that the size of such an impedance contrast is probably not correctly reflected in the resulting earth models. However, the depth to the isotherm roughly agrees with the depth to the velocity reduction of about 40–45 km underneath stations HOT01, 27 and 28. Beneath HOT18N, HOT24WSW and HOT21 and 22, the isotherm is proposed to lie at a depth of roughly 50 km, but the indication of a velocity inversion occurs at 35–40 km depth. The depth estimate of the isotherm depends upon

Moho depth estimates, which are deeper in Kaban *et al.* (2002) than found here or in Darbyshire *et al.* (2000b), thus a somewhat shallower position of the isotherm might be conceivable.

CONCLUSION

Teleseismic receiver function analysis as a tool for studying crustal and upper mantle structure is difficult to use in Iceland due to weak seismic signals from the subsurface, high crustal heterogeneity and noise-contaminated recordings. Converted and multiply reflected phases from deep and shallow interfaces interfere and introduce uncertainty in the phase identification. The testing of a variety of alternative crustal models is, therefore, necessary; the assessment of the respective quality of the model being subjective. Comparison of the results of this study with other studies has shown that any quantitative interpretation of the 1-D models depends critically upon the methodological approach and subjectivity of the interpretation. Instead, I restricted the interpretation of the receiver functions to qualitative statements supported by the results of this study and the independent receiver function studies of DA and DF. On this basis the following conclusions can be drawn:

(1) The results for many stations in West and East Iceland as well as in northern central Iceland are inconclusive, probably indicating pronounced structural heterogeneity of the crust.

(2) The change in seismic gradient between the upper and lower crust is properly reflected in the receiver function models. It accounts for much of the receiver function signal.

(3) The style of the crust–mantle transition varies drastically across Iceland from a first-order velocity discontinuity to hardly being discernible. A classical seismic Moho does not explain the majority of the receiver functions.

(4) A reduction of *S*-wave velocities in the upper mantle is eventually supported by the receiver functions. It might signal a shallow asthenosphere.

Hence, the use of the present teleseismic receiver function studies for unravelling the details of the crust–mantle transition underneath Iceland remains limited. Specifically, depth estimates of the Moho should be used in further studies with great care. For more detailed and quantitative results, future teleseismic receiver function studies should seek to collect a large number of high-quality seismic events clustering in narrow backazimuthal and epicentral regions. This would eventually allow identification and even modelling of non-1-D structure that is certainly present, such as dipping layers or anisotropic effects. The inversion of receiver function stacks thus obtained should be constrained in a joint modelling approach as proposed by Du *et al.* (2002) by robust information on absolute seismic velocities in the immediate vicinity of the stations using surface wave and seismic refraction results. Intensive forward modelling is vital to understand the provenance of phases, to simplify the velocity models obtained, and to assess the robustness of discontinuities. Finally, it would be advantageous to find a way to quantitatively measure the quality of the fit to relevant signal in order to avoid biasing of the results by anticipation of certain structures.

ACKNOWLEDGMENTS

I would like to thank the HOTSPOT group, G. R. Foulger, M. J. Pritchard, B. R. Julian, R. M. Allen, B. H. Bergsson, P. Erlendsson, S. Jakobsdóttir, W. J. Morgan, G. Nolet, S. Ragnarsson, R. Stefansson and K. Vogfjörd, for providing the data. I am indebted to Z. J. Du for computational support. I greatly acknowledge fruitful discussions with I. Th. Bjarnason, F. A. Darbyshire, N. R. Goulty and R. C. Searle. Thorough reviews by B. Brandsdóttir, R. White and R. Evans greatly helped to improve the manuscript. I received funding for this project from the German Academic Exchange Service (DAAD/HSP III-Programme) and the European Commission under TMR grant ERBFMBICT983266.

REFERENCES

Allen, R.M. *et al.,* 1999. The thin hot plume beneath Iceland, *Geophys. J. Int.,* **137,** 51–63.

Ammon, C.J., 1991. The isolation of receiver effects from teleseismic P waveforms, *Bull. seism. Soc. Am.,* **81,** 2504–2510.

Ammon, C.J., Randall, G.E. & Zandt, G., 1990. On the nonuniqueness of receiver function inversions, *J. geophys. Res.,* **95,** 15 303–15 318.

Angenheister, G. *et al.*, 1980. Reykjanes Ridge Iceland Seismic Experiment (RRISP 77), *J. Geophys.,* **47,** 228–238.

Beblo, M. & Björnsson, A., 1980. A model of electrical resistivity beneath NE-Iceland, correlation with temperature, *J. Geophys.,* **47,** 184–190.

Berteussen, K.A., 1977. Moho depth determinations based on spectral ratio analysis of NORSAR long period P waves, *Phys. Earth planet. Inter.,* **15,** 13–27.

Bjarnason, I.Th., 1999. How thick is the lithosphere in Iceland? How large is the velocity inversion in the asthenosphere and what does it mean? (abstract), *EOS, Trans. Am. geophys. Un.,* **80,** 645.

Bjarnason, I.Th., Menke, W., Flóvenz, Ó.G. &Caress, D., 1993. Tomographic image of the mid-Atlantic plate boundary in southwestern Iceland, *J. geophys. Res.,* **98,** 6607–6622.

Bjarnason, I.Th., Menke, W. & Flóvenz, Ó.G., 1994. Reply (to Gudmundsson 1994), *J. geophys. Res.,* **99,** 17 915–17 917.

Bown, J.W. & White, R.S., 1994. Variation with spreading rate of oceanic crustal thickness and geochemistry, *Earth planet. Sci. Lett.,* **121,** 435–449.

Brandsdóttir, B., Menke, W., Einarsson, P., White, R.S. & Staples, R.K., 1997. Faroe-Iceland Ridge Experiment 2. Crustal structure of the Krafla central volcano, *J. geophys. Res.,* **102,** 7867–7886.

Carlson, R.L. & Herrick, C.N., 1990. Densities and porosities in the oceanic crust and their variations with depth and age, *J. geophys. Res.,* **95,** 9153–9170.

Cassidy, J.F., 1992. Numeric experiments in broadband receiver function analysis, *Bull. seism. Soc. Am.,* **82,** 1453–1474.

Darbyshire, F.A., Bjarnason, I.Th., White, R.S. & Flóvenz, Ó.G., 1998. Crustal structure above the Iceland mantle plume imaged by the ICEMELT refraction profile, *Geophys. J. Int.,* **135,** 1131–1149.

Darbyshire, F.A., Priestley, K.F., White, R.S., Stefánsson, R., Gudmundsson, G.B. & Jakobsdóttir, S.S., 2000a. Crustal structure of central and northern Iceland from analysis of teleseismic receiver functions, *Geophys. J. Int.,* **143,** 163–184.

Darbyshire, F.A., White, R.S. & Priestley, K.F., 2000b. Structure of the crust and uppermost mantle in Iceland from a combined seismic and gravity study, *Earth planet. Sci. Lett.,* **181,** 409–428.

Du, Z.J. & Foulger, G.R., 1999. The crustal structure beneath the northwest fjords, Iceland, from receiver functions and surface waves, *Geophys. J. Int.,* **139,** 419–432.

Du, Z.J. & Foulger, G.R., 2001. Variations in the crustal structure across central Iceland, *Geophys. J. Int.,* **145,** 246–264.

Du, Z.J. *et al.,* 2002. Crustal structure beneath western and eastern Iceland from surface waves and receiver functions, *Geophys. J. Int.,* **149,** 349–363.

Eysteinsson, H. & Hermance, J.F., 1985. Magnetotelluric measurements across the eastern neovolcanic zone in south Iceland, *J. geophys. Res.,* **90,** 10 093–10 103.

Flóvenz, Ó.G., 1980. Seismic structure of the Icelandic crust above Layer Three and the relation between body wave velocity and the alteration of the basaltic crust, *J. Geophys.,* **47,** 211–220.

Flóvenz, Ó.G. & Gunnarsson, K., 1991. Seismic crustal structure in Iceland and surrounding area, *Tectonophysics,* **189,** 1–17.

Flóvenz, Ó.G. & Sæmundsson, K., 1993. Heat flow and geothermal processes in Iceland, *Tectonophysics,* **225,** 123–138.

Gebrande, H., Miller, H. & Einarsson, P., 1980. Seismic structure of Iceland along RRISP-Profile I, *J. Geophys.,* **47,** 239–249.

Gudmundsson, Ó., 1994. Comment on 'Tomographic image of the Mid-Atlantic plate boundary in southwestern Iceland' by I.T. Bjarnason, W. Menke, Ó.G. Flóvenz, and D. Caress, *J. geophys. Res.,* **99,** 17 909–17 914.

Gudmundsson, Ó., 2003. The dense root of the Iceland crust, *Earth planet. Sci. Lett.,* **206,** 427–440.

Jóhannesson, H. & Sæmundsson, K., 1998. Geological map of Iceland, 1:500 000, Tectonics, Icelandic Institute of Natural History, Reykjavík.

Jones, C.H. & Phinney, R.A., 1998. Seismic structure of the lithosphere from teleseismic converted arrivals observed at small arrays in the southern Sierra Nevada and vicinity, California, *J. geophys. Res.,* **103,** 10 065–10 090.

Kaban, M.K., Flóvenz, Ó.G. & Pálmason, G., 2002. Nature of the crust-mantle transition zone and the thermal state of the upper mantle beneath Iceland from gravity modelling, *Geophys. J. Int.,* **149,** 281–299.

Kosarev, G., Kind, R., Sobolev, S.V., Yuan, X., Hanka, W. & Oreshin, S., 1999. Seismic evidence for a detached Indian lithospheric mantle beneath Tibet, *Science,* **283,** 1306–1309.

Langston, C.A., 1979. Structure under Mount Rainier, Washington, inferred from teleseismic body waves, *J. geophys. Res.,* **84,** 4749–4762.

Li, X., Kind, R., Priestley, K., Sobolev, S.V., Tilmann, F., Yuan, X. & Weber, M., 2000. Mapping the Hawaiian plume conduit with converted seismic waves, *Nature,* **405,** 938–941.

Menke, W., Brandsdóttir, B., Jakobsdóttir, S. & Stefánsson, R., 1994. Seismic anisotropy in the crust at the Mid-Atlantic plate boundary in south-west Iceland, *Geophys. J. Int.,* **119,** 783–790.

Menke, W., Brandsdóttir, B., Einarsson, P. & Bjarnason, I.Th., 1996. Reinterpretation of the RRISP-77 Iceland shear-wave profiles, *Geophys. J. Int.,* **126,** 166–172.

Menke, W., West, M., Brandsdóttir, B. & Sparks, D., 1998. Compressional and shear velocity structure of the lithosphere in northern Iceland, *Bull. seism. Soc. Am.,* **88,** 1561–1571.

Pálmason, G., 1973. Kinematics and heat flow in a volcanic rift zone, with application to Iceland, *Geophys. J.R. astr. Soc.,* **33,** 451–481.

Sæmundsson, K., 1979. Outline of the geology of Iceland, *Jökull,* **29,** 7–28.

Schlindwein, V., 2001. Azimuthal variation of the P phase in Icelandic receiver functions, *Geophys. J. Int.,* **144,** 221–230.

Staples, R.K., White, R.S., Brandsdóttir, B., Menke, W., Maguire, P.K.H. & McBride, J.H., 1997. Färoe-Iceland Ridge Experiment 1. Crustal structure of northeastern Iceland, *J. geophys. Res.,* **102,** 7849–7866.

Weir, N.R.W., White, R.S., Brandsdóttir, B., Einarsson, P., Shimamura, H., Shiobara, H. & The RISE Fieldwork Team, 2001. Crustal structure of the northern Reykjanes Ridge and Reykjanes Peninsula, southwest Iceland, *J. geophys. Res.,* **106,** 6347–6368.

Wolfe, C.J., Bjarnason, I.Th., VanDecar, J.C. & Solomon, S.C., 1997. Seismic structure of the Iceland mantle plume, *Nature,* **385,** 245–247.